research papers

Effects of fluoro substitution on 4-bromodiphenyl ether (PBDE 3)

J. Klösener,[a,b] D. C. Swenson,[c] L. W. Robertson[a] and G. Luthe[a,c,d]*

[a]Department of Occupational and Environmental Health, University of Iowa, 100 Oakdale Campus # 124 IREH, Iowa City, IA 52242-5000, USA, [b]Institute for Life Science and Technology, Saxion University of Applied Sciences, Enschede, The Netherlands, [c]Department of Chemistry, University of Iowa, Iowa City, IA, USA, and [d]University of Bremen, Institute for Inorganic and Physical Chemistry, Bremen, Germany

Correspondence e-mail:
gregor-luthe@uiowa.edu

It is our hypothesis that fluoro substitution provides a powerful tool to modulate the desired characteristics and to increase the specificity of studies of structure–activity relationships. 4-Bromodiphenyl ether (PBDE 3) and its five corresponding monofluorinated analogues (F-PBDEs 3) have been synthesized and fully characterized (using ^{1}H, ^{13}C and ^{19}F NMR spectroscopy, and mass spectrometry). The accurate structure from X-ray crystal analysis was compared with iterative calculations using semi-empirical self-consistent field molecular-orbital (SCF-MO) models. The compounds studied were 4-bromodiphenyl ether (PBDE 3), the ^{13}C$_6$-isotopically labeled PBDE 3 (^{13}C$_6$-PBDE 3) and 2-fluoro-4-bromodiphenyl ether (3-2F), 2′-fluoro-4-bromodiphenyl ether (3-2′F), 3-fluoro-4-bromodiphenyl ether (3-3F), 3′-fluoro-4-bromodiphenyl ether (3-3′F), and 4′-fluoro-4-bromodiphenyl ether (3-4′F). Solid-state intermolecular interactions for PBDE 3 and the F-PBDEs 3 isomers are dominated by weak C—H(F,Br)$\cdots\pi$ and C—H$\cdots$F interactions. The C—F bond lengths varied between 1.347 (2) and 1.362 (2) Å, and the C4—Br bond length between 1.880 (3) and 1.904 (2) Å. These bond lengths are correlated with electron-density differences, as determined by ^{13}C shifts, but not with the strength of the C—F couplings. The interior ring angles of *ipso*-fluoro substitution increased (121.9–124.0°) as a result of hyperconjugation, a phenomenon also predicted by the calculation models. An attraction between the vicinal fluoro and halo substituents (observed in fluoro substituted chlorobiphenyls) was not observed for the bromo substituted F-PBDEs. The influence of a fluoro substituent on the conformation was only observable in PBDEs with di-*ortho* substitution. Calculated and observed torsion angles showed a positive correlation with increasing van der Waals radii and/or the degree of substitution for mono- to tetra-fluoro, chloro, bromo and methyl substitutions in the *ortho* positions of diphenyl ether. These findings utilizing F-tagged analogues presented here may prove fundamental to the interpretation of the biological effects and toxicities of these persistent environmental pollutants.

1. Introduction

Polybrominated diphenyl ethers (PBDEs) constitute a class of 209 individual congeners, distinguishable by the degree of bromination (mono- to deca-) and the position of bromine(s) in the rings, see Fig. 1. PBDEs are incorporated as flame-retardants in materials using an 'additive' process and thus may slowly volatilize into the environment during the product's lifetime (Sjödin *et al.*, 2001; Bromine Science and

Table 1
^{13}C chemical shifts δ (p.p.m.) relative to TMS, the ^{13}C–^{19}F couplings J (Hz) over n bonds of all C atoms in PBDE 3 and F-PBDE 3 congeners.

Numbering is according to the BZ or the BZL systems; BZ 0 refers to the non-substituted diphenyl ether.

BZ/BZL No.	Coupling	C1	C2	C3	C4	C5	C6	C1′	C2′	C3′	C4′	C5′	C6′
0		156.9	119.2	130.1	123.9	130.1	119.2	156.9	119.2	130.1	123.9	130.1	119.2
3		156.8	120.6	132.9	115.8	132.9	120.6	156.9	119.2	130.1	123.9	130.1	119.2
3-2F		143.5	154.3	120.8	116.2	128.0	122.9	157.0	117.7	130.0	123.8	130.0	117.7
	^{n}J(C,F)	11.32	253.60	21.13	8.30	3.77	1.51						
		(n = 2)	(n = 1)	(n = 2)	(n = 3)	(n = 4)	(n = 3)						
3-3F		158.5	107.1	159.7	102.1	133.9	115.3	156.0	119.8	130.3	124.7	130.3	119.8
	^{n}J(C,F)	9.81	25.66	247.56	21.13	1.51	3.77						
		(n = 3)	(n = 2)	(n = 1)	(n = 2)	(n = 3)	(n = 4)						
3-2′F		156.8	119.0	132.8	115.7	132.8	119.0	143.3	154.0	117.4	125.6	122.3	125.0
	^{n}J(C,F)							11.32	249.07	18.11	6.79	0.75	3.77
								(n = 2)	(n = 1)	(n = 2)	(n = 3)	(n = 4)	(n = 3)
3-3′F		155.7	121.7	133.7	116.7	133.7	121.7	158.5	106.4	163.7	110.5	130.8	114.2
	^{n}J(C,F)							10.57	24.91	247.56	21.13	9.81	3.02
								(n = 3)	(n = 2)	(n = 1)	(n = 2)	(n = 3)	(n = 4)
3-4′F		157.1	120.0	132.9	115.7	132.9	120.0	152.5	120.9	116.7	159.2	116.7	120.9
	^{n}J(C,F)							2.26	8.30	23.40	242.28	23.40	8.30
								(n = 4)	(n = 3)	(n = 2)	(n = 1)	(n = 2)	(n = 3)

Environment Forum, 2003; Nordic Council of Ministers, 1998). The PBDEs are now ubiquitous contaminants and due to their lipophilic character, high bioavailability and slow elimination they bio-accumulate in the body and bio-magnify in the food web (Meironyte *et al.*, 1999; Lind *et al.*, 2002; Hites, 2004; Bergman *et al.*, 1999; Johanson-Restrepo *et al.*, 2005; Hites *et al.*, 2005). As PBDE levels increase, so does the public health threat; there is concern over their potential for liver toxicity, disruption of thyroid hormone homeostasis, neurotoxicity, reproductive and developmental toxicity, and carcinogenicity.

Knowledge of PBDE conformations and homologies to examine the potential models for ligand binding, and substrate specificity marks the beginning of our understanding of the biological activity of PBDEs as agonists, antagonists and substrates. Currently this knowledge is extremely limited and controversial. For a complete overview of biological transcription factors activated by PBDEs, see Luthe, Schut *et al.* (2007). The conformations of diphenyl ethers are described by the torsional angles (φ_1 and φ_2) between the C1—O—C1′ plane and planes of the phenyl rings. The angles are defined as
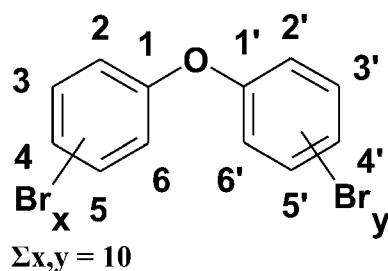
Figure 1
Numbering of PBDEs according to the Ballschmiter–Zell (BZ) nomenclature.

positive when the rotation is clockwise looking down the C4—C1 and C4′—C1′ axes toward the oxygen. There are four possible conformations of diphenyl ethers: planar ($\varphi_1 = \varphi_2 = 0°$), butterfly ($\varphi_1 = \varphi_2 = 90°$), skew ($\varphi_1 = 0°$, $\varphi_2 = 90°$) and twist ($\varphi_1, \varphi_2 > 0°$). A variety of experimental and theoretical studies have shown that the unsubstituted diphenyl ether itself has a twist conformation in that φ_1 and φ_2 lie in the range 25–50° (Schaefer *et al.*, 1988). Choudhury *et al.* (2004) determined the two different polymorphs of diphenyl ether to be C—H···π-mediated polymeric forms. PBDE congeners adopt a skew or twist conformation depending on the number of *ortho*-bromo substituents (Nevalainen & Rissanen, 1994). One approach to gain information about the three-dimensional structure of PBDEs is *via* X-ray analysis of single crystals or solid-state NMR spectroscopy; another is to calculate geometries under ideal vacuum conditions. Each approach has drawbacks in modeling the molecular structure in solution. Relatively few crystal structures of PBDEs have been reported or calculated to help understand quantitative structure–activity relationships (QSAR) in biological systems. 4-Bromodiphenyl ether (PBDE 3) is the fundamental PBDE and is ideal for studying conformational changes to gain general information about this group of important compounds.

It is our hypothesis that fluoro substitution (so-called F-tagging) can be employed to study the biological activity of a given PBDE congener by altering the electron density and blocking specific positions in a desired manner without drastically altering the three-dimensional structure. Fluoro substitutions result in analogues closely resembling the corresponding parent compounds in shape and polarity. This is due to several distinctive characteristics of the fluoro substituent; *e.g.* mimicking the size of the hydrogen that it 'replaces' in the present study. F-tagged analogues provide a powerful tool for increasing the specificity of QSAR studies and will

Table 2
Bond lengths (Å), bond angles (°) and torsion angles (°) observed by X-ray compared with values from the SCF-MO calculation (italics).

Structure specifications Bond lengths (Å)	PBDE 3 and F-PBDEs 3					
	3	3-2F	3-2'F	3-3F	3-3'F	3-4'F
Br—C4	1.896 (3) *1.872*	1.897 (2) *1.872*	1.903 (2) *1.872*	1.880 (3) *1.871*	1.904 (2) *1.872*	1.897 (3) *1.872*
F—C	–	1.349 (1) *1.351*	1.347 (2) *1.351*	1.357 (3) *1.352*	1.362 (2) *1.354*	1.354 (3) *1.355*
C1—C2	1.401 (4) *1.399* *1.405*	1.378 (2) *1.418*	1.384 (3) *1.405* *1.399*	1.392 (3) *1.394*	1.382 (3) *1.400* *1.404*	1.383 (4) *1.399* *1.405*
C1—C6	1.396 (3) *1.399* *1.405*	1.385 (2) *1.397*	1.379 (3) *1.405* *1.399*	1.400 (4) *1.407*	1.379 (3) *1.400* *1.404*	1.379 (4) *1.399* *1.405*
C2—C3	1.377 (4) *1.393* *1.391*	1.383 (1) *1.405*	1.381 (3) *1.390* *1.393*	1.377 (4) *1.409*	1.386 (3) *1.392* *1.392*	1.392 (4) *1.393* *1.399*
C3—C4	1.389 (3) *1.398* *1.400*	1.383 (2) *1.395*	1.383 (3) *1.400* *1.397*	1.374 (4) *1.411*	1.382 (3) *1.411*	1.390 (4) *1.395*
C4—C5	1.393 (4) *1.398* *1.400*	1.382 (3) *1.398*	1.378 (4) *1.400* *1.397*	1.397 (4) *1.401*	1.376 (3) *1.399* *1.391*	1.374 (4) *1.399* *1.398*
C5—C6	1.385 (4) *1.393* *1.391*	1.391 (3) *1.392*	1.392 (3) *1.390* *1.393*	1.376 (4) *1.387*	1.384 (3) *1.392* *1.392*	1.386 (4) *1.399* *1.398*
C1'—C6'	1.396 (3) *1.400* *1.402*	1.378 (2) *1.403*	1.380 (3) *1.399* *1.400*	1.380 (4) *1.400*	1.384 (3) *1.404* *1.402*	1.388 (4) *1.400* *1.403*
C1'—C2'	1.386 (4) *1.402* *1.400*	1.385 (2) *1.403*	1.381 (3) *1.415* *1.400*	1.373 (4) *1.400*	1.391 (3) *1.397* *1.402*	1.381 (4) *1.400* *1.403*
C2'—C3'	1.392 (4) *1.394* *1.393*	1.389 (3) *1.393*	1.375 (3) *1.408* *1.394*	1.396 (5) *1.394*	1.377 (3) *1.407* *1.394*	1.385 (4) *1.390* *1.390*
C3'—C4'	1.395 (4) *1.395* *1.396*	1.389 (3) *1.395*	1.383 (3) *1.391* *1.396*	1.379 (5) *1.395*	1.371 (3) *1.407* *1.396*	1.376 (4) *1.408* *1.408*
C4'—C5'	1.389 (4) *1.395* *1.396*	1.376 (3) *1.395*	1.385 (4) *1.396* *1.396*	1.382 (5) *1.395*	1.385 (3) *1.393* *1.396*	1.376 (4) *1.408* *1.408*
C5'—C6'	1.388 (4) *1.393* *1.394*	1.395 (2) *1.393*	1.390 (3) *1.392* *1.394*	1.385 (4) *1.394*	1.397 (3) *1.392* *1.394*	1.395 (4) *1.390* *1.390*
C1—O	1.376 (3) *1.389*	1.389 (18) *1.386*	1.386 (2) *1.391*	1.364 (3) *1.386*	1.393 (2) *1.391*	1.395 (4) *1.390*
C1'—O	1.386 (3) *1.394*	1.400 (2) *1.396*	1.389 (2) *1.391*	1.410 (3) *1.396*	1.384 (3) *1.391*	1.384 (3) *1.393*
C2—C1—C6	120.1 (2) *121.0*	119.24 (13) *120.2*	120.87 (18) *121.1*	119.5 (2) *121.1*	121.24 (19) *121.1*	121.3 (3) *121.0*
C6—C1—O	124.4 (2) *123.8* *115.2*	120.80 (14) *124.0*	123.96 (17) *114.8* *124.1*	126.3 (2) *124.0*	118.8 (2) *115.5* *123.3*	121.1 (3) *115.1* *123.7*
C2—C1—O	115.4 (2) *123.8* *115.2*	119.93 (13) *115.7*	115.16 (17) *114.8* *124.1*	114.2 (2) *114.8*	119.88 (18) *115.5* *123.3*	117.5 (3) *115.1* *123.7*
C3—C2—C1	120.2 (2) *119.2* *119.2*	121.95 (10) *119.3*	119.80 (19) *119.0* *119.2*	118.8 (2) *119.2*	119.45 (19) *119.2* *119.2*	119.3 (3) *119.2* *119.2*
C2—C3—C4	119.5 (2) *120.3* *120.4*	117.75 (13) *119.9*	119.43 (18) *120.3* *120.4*	122.9 (2) *120.4*	119.0 (2) *120.3* *120.4*	118.8 (3) *120.3* *120.4*
C5—C4—C3	120.8 (2) *120.0*	121.95 (16) *120.5*	120.92 (19) *120.0*	117.9 (2) *118.8*	121.63 (19) *120.1*	121.7 (3) *120.3*
C4—C5—C6	119.9 (2) *120.4* *120.4*	118.88 (17) *120.3*	119.7 (2) *120.3* *120.4*	120.9 (2) *121.5*	119.29 (19) *120.3* *120.4*	119.3 (3) *120.3* *120.4*
C5—C6—C1	119.5 (2) *119.1* *119.2*	120.23 (16) *119.9*	119.29 (18) *119.2* *119.2*	120.1 (2) *119.0*	119.4 (2) *119.0* *119.2*	119.6 (3) *119.2* *119.2*

also diminish the study costs by reducing the number of study compounds needed for interpretable results. Preliminary studies on monofluorinated analogues of polycyclic aromatic hydrocarbons (F-PAHs; Luthe et al., 2002), polychlorinated biphenyls (F-PCBs; Luthe, Jacobus & Robertson, 2007; Luthe, Swenson & Robertson, 2007) and polybrominated diphenylethers (F-PBDEs; Luthe, Leonards, Reijerink, Liu, Johansen & Robertson, 2006) have been very promising

To test this hypothesis, we present here the synthesis and determination of the crystal structures of a series of the possible monofluorinated isomers (F-PBDEs 3) of the fundamental PBDE 3 isomer, i.e. 2-fluoro-4-bromodiphenyl ether (3-2F), 2'-fluoro-4-bromodiphenyl ether (3-2'F), 3-fluoro-4-bromodiphenyl ether (3-3F), 3'-fluoro-4-bromodiphenyl ether (3-3'F) and 4'-fluoro-4-bromodiphenyl ether (3-4'F). In the nomenclature, the first number refers to the corresponding PBDE, the second indicates the position of the substituent, e.g. fluorine, with the bromo substituent having the highest priority. This Ballschmiter–Zell–Luthe (BZL) system (Luthe, Leonards, Reijerink, Liu, Johansen & Robertson, 2006; Luthe, Schut et al., 2006; Luthe, Swenson & Robertson 2007) corresponds to the broadly used BZ system (Ballschmiter & Zell, 1980), see Fig. 1. As the conformations of these flexible study compounds are influenced by intermolecular interactions in the solid state, we compare and discuss the molecular conformations determined by X-rays with those calculated employing SCF-MO calculation methods. In addition, we used calculations to compare the effects of di- to tetrafluoro substitutions in the ortho-postions of diphenyl ether with chloro, bromo and methyl substitutions. This is another step in our long-term aim of exploring the potential of F-tagging to investigate biological endpoints.

Table 2 (continued)

Structure specifications Bond lengths (Å)	PBDE 3 and F-PBDEs 3					
	3	3-2F	3-2'F	3-3F	3-3'F	3-4'F
C6'—C1'—C2'	120.8 (2)	121.65 (15)	119.11 (19)	122.1 (3)	121.35 (19)	120.9 (3)
	121.4	*121.5*	*120.6*	*121.5*	*121.7*	*121.4*
C6'—C1'—O	122.8 (2)	122.46 (16)	119.48 (18)	121.8 (3)	123.73 (18)	122.7 (3)
	122.5	*122.7*	*122.2*	*116.4*	*115.3*	*115.9*
	115.9	*115.6*	*117.9*	*121.8*	*122.7*	*122.5*
C2'—C1'—O	116.1 (2)	115.88 (16)	121.24 (19)	115.8 (3)	114.91 (17)	116.3 (3)
	115.9	*115.6*	*117.0*	*116.4*	*122.8*	*122.8*
	122.5	*122.7*	*122.4*	*121.8*	*117.0*	*115.9*
C3'—C2'—C1'	119.5 (2)	118.77 (16)	121.9 (2)	118.6 (3)	117.2 (2)	120.1 (3)
	118.7	*118.7*	*119.0*	*118.7*	*118.3*	*119.3*
	118.9	*118.8*		*118.8*		*119.3*
C4'—C3'—C2'	120.5 (2)	120.46 (16)	118.8 (2)	120.2 (3)	124.0 (2)	118.7 (3)
	120.4	*120.3*	*119.9*	*120.3*	*120.7*	*119.7*
	120.5	*120.5*		*120.4*		*119.8*
C3'—C4'—C5'	119.1 (3)	119.67 (15)	120.2 (2)	120.1 (2)	117.3 (2)	122.2 (3)
	120.2	*120.2*	*120.7*	*120.3*	*119.4*	*120.5*
C4'—C5'—C6'	121.2 (2)	120.77 (16)	120.2 (2)	120.4 (3)	121.4 (2)	119.1 (3)
	120.4	*120.3*	*120.3*	*120.3*	*121.0*	*119.7*
	120.5	*120.5*		*120.4*		*119.8*
C5'—C6'—C1'	118.9 (2)	118.67 (16)	119.8 (2)	118.6 (3)	118.7 (2)	119.0 (3)
	118.7	*118.7*	*119.6*	*118.7*	*118.8*	*119.3*
	118.9	*118.8*		*118.8*		*119.3*
F—C—C		F—C2—C1	F—C2'—C1'	F—C3—C2	F—C3'—C2'	F—C4'—C3'
		118.85(11)	118.56(19)	117.7(2)	117.15(19)	119.1(3)
		120.6	*120.7*	*118.0*	*119.5*	*119.9*
F—C—C		F—C2—C3	F—C2'—C3'	F—C3—C4	F—C3'—C4'	F—C4'—C5'
		119.19 (12)	119.52 (19)	119.4 (2)	118.82 (19)	118.7 (3)
		120.1	*120.3*	*121.6*	*119.9*	*119.9*
Br—C4—C3	120.3 (2)	119.12 (12)	119.85 (15)	121.0 (2)	119.35 (16)	119.4 (2)
	120.0	*119.6*	*120.0*	*122.8*	*120.0*	*120.0*
Br—C4—C5	118.90 (18)	118.92 (13)	119.22 (16)	121.1 (2)	119.01 (15)	118.8 (2)
	119.9	*120.0*	*120.0*	*118.4*	*119.9*	*119.9*
C1'—O—C1—C6(2)	−25.9 (3)	−102.7 (2)	−4.1 (3)	172.2 (2)	94.9 (2)	55.9 (4)
	158.7 (2)	79.5 (3)	175.13 (18)	−8.9 (4)	−88.1 (2)	−127.9 (3)
		71 (2) (C'')				
		−109 (2) (C'')				
	155.7	*152.4*	*162.3*	*164.6*	*147.8*	*155.5*
	−28.0	*−31.8*	*−20.4*	*−18.0*	*−37.0*	*−28.2*
C2'(6')—C1'—O—C1	142.6 (2)	21.3 (4)	−108.7 (2)	130.0 (3)	6.6 (3)	−154.5 (3)
	−42.9 (3)	−160.1 (3)	76.1 (3)	−55.2 (4)	−173.55 (18)	29.2 (4)
		28 (5) (C'')				
		−157 (4) (C'')				
	139.6	*142.2*	*129.2*	*130.5*	*148.8*	*139.1*
	−45.8	*−43.0*	*−57.0*	*−55.5*	*−35.8*	*−46.4*
C1—O—C1'	121.09 (18)	115.96 (12)	118.93 (15)	120.9 (2)	118.05 (15)	118.1 (2)
	116.9	*116.7*	*116.6*	*117.0*	*117.1*	*116.8*

2. Experimental

2.1. Syntheses, and ^{1}H, ^{13}C and ^{19}F NMR characterization

Information on the syntheses of the compounds is given in the supplementary material.[1] The synthesis procedure, chemicals, synthesis monitoring, clean-up, yields and gas chromatograph coupled mass spectrometry (GC-MS) characterization have all been deposited.

PBDE 3, ^{13}C$_6$-PBDE 3 and F-PBDEs 3 were characterized by means of proton (^{1}H), carbon (^{13}C), fluorine (^{19}F) NMR spectroscopy, and ^{13}C ^{1}H correlated spectroscopy (COSY). The ^{1}H and ^{13}C NMR spectra were recorded on a 300 MHz NMR spectrometer (Bruker, Billerica, MA, USA), using CDCl3 as the solvent. Chemical shifts (δ) are given in p.p.m. relative to TMS and coupling constants, J, in Hz. The ^{13}C NMR results are listed in Table 1; those of the ^{1}H NMR are presented in §3.2. ^{19}F NMR spectra were obtained with a 5 mm QNP probe, operating at 282.4 MHz. Chemical shifts were calibrated against hexafluorobenzene as a standard. An overview of the shifts, couplings and images of the COSY spectra are available in the supplementary material.

2.2. Molecular-orbital calculations

To calculate the conformation of the PBDE 3 and the corresponding F-PBDEs 3, semiempirical SCF-MO calculations using an AM1 Hamiltonian basis set 3-21G (Dewar et al., 1985) with the Spartan '06 package (Shao et al., 2006) were carried out on a Quad 2.5 GHz Power Mac G5 with a PCI express graphics card. Table 2 gives an overview of the calculated bond lengths, interior angles and the torsion angles, and Table 3 of the experimental details. The heats of formation were calculated using a starting geometry similar to the optimized geometry. The use of symmetry constraints enhanced the convergence compared with completely unconstrained runs. The iterations and cut-offs are 18, 4.1868×10^{-4} (PBDE 3), 67, 5.862×10^{-4} (3-2F), 47, 6.699×10^{-4} (3-2'F), 20, 7.536×10^{-4} (3-3F), 18, 7.536×10^{-4} (3-3'F), and 18, 8.374×10^{-4} kJ mol^{-1} (3-4'F). The conformations of diphenyl ethers are described by the torsional angles (φ_1 and φ_2) between the C1—O—C1' plane and the planes of the phenyl rings. The angles are defined as positive when the rotation is clockwise looking down the C4—C1 and C4'—C1' direction toward the oxygen. The conformations were calculated for fluoro, chloro, bromo and methyl substitutents. The cut-off was defined by a threshold of 5.024×10^{-4} kJ mol^{-1}. The observed and calculated torsion angles (C1'—O—C1—C6 and C2'—C1'—O—C1), the C1—O—C1' angles and the iterations of the calculations are listed in Table 4.

---

[1] Supplementary data for this paper are available from the IUCr electronic archives (Reference: BK5067). Services for accessing these data are described at the back of the journal.

Table 3
Experimental details for PBDE 3 and the five F-PBDE 3 isomers.

	PBDE 3 and F-PBDEs 3					
	3	3-2F	3-2′F	3-3F	3-3′F	3-4′F
Crystal data						
Chemical formula	$C_{12}H_9BrO$	$C_{12}H_8BrFO$	$C_{12}H_8BrFO$	$C_{12}H_8BrFO$	$C_{12}H_8BrFO$	$C_{12}H_8BrFO$
M_r	249.10	267.09	267.09	267.09	267.09	267.09
Cell setting, space group	Monoclinic, Cc	Orthorhombic, $P2_12_12_1$	Monoclinic, $C2/c$	Orthorhombic, $Pca2_1$	Monoclinic, $P2_1/n$	Monoclinic, Cc
Temperature (K)	150 (2)	150 (2)	150 (2)	150 (2)	150 (2)	150 (2)
a, b, c (Å)	23.628 (3), 7.5461 (9), 5.8066 (7)	5.8708 (7), 9.0974 (10), 19.396 (2)	23.752 (3), 4.3622 (5), 21.357 (3)	14.9203 (16), 11.6841 (13), 5.8727 (7)	5.9477 (7), 9.0635 (10), 19.481 (2)	6.0033 (7), 23.186 (3), 7.4329 (8)
β (°)	97.919 (5)	90.00	110.762 (5)	90.00	94.030 (5)	91.480 (5)
V (Å³)	1025.4 (2)	1035.9 (2)	2069.1 (5)	1023.8 (2)	1047.6 (2)	1034.3 (2)
Z	4	4	8	4	4	4
D_x (Mg m⁻³)	1.614	1.713	1.715	1.733	1.694	1.715
Radiation type	Mo $K\alpha$	Mo $K\alpha$	Mo $K\alpha$	Mo $K\alpha$	Mo $K\alpha$	Mo $K\alpha$
μ (mm⁻¹)	3.97	3.95	3.95	4.00	3.90	3.96
Crystal form, color	Plate, colorless	Irregular prism, colorless	Plate, colorless	Plate, colorless	Needle, colorless	Plate, colorless
Crystal size (mm)	$0.36 \times 0.24 \times 0.07$	$0.34 \times 0.31 \times 0.19$	$0.19 \times 0.16 \times 0.06$	$0.45 \times 0.44 \times 0.08$	$0.38 \times 0.08 \times 0.07$	$0.33 \times 0.16 \times 0.03$
Melting point (K)	290	278	268	268	289	293
Data collection						
Diffractometer	Nonius KappaCCD	Nonius KappaCCD	Nonius KappaCCD	Nonius KappaCCD	Nonius KappaCCD	Nonius KappaCCD
Data collection method	CCD φ and ω scans	CCD φ and ω scans	CCD φ and ω scans	CCD φ and ω scans	CCD φ and ω scans	CCD φ and ω scans
Absorption correction	Multi-scan (based on symmetry-related measurements)	Multi-scan (based on symmetry-related measurements)	Multi-scan (based on symmetry-related measurements)	Multi-scan (based on symmetry-related measurements)	Multi-scan (based on symmetry-related measurements)	Multi-scan (based on symmetry-related measurements)
T_{min}	0.329	0.315	0.520	0.267	0.318	0.355
T_{max}	0.769	0.473	0.797	0.741	0.772	0.891
No. of measured, independent and observed reflections	11 708, 2310, 2216	21 969, 2373, 2293	19 505, 2367, 2029	15 796, 2327, 2190	21 638, 2390, 1891	9753, 2289, 2170
Criterion for observed reflections	$I > 2\sigma(I)$	$I > 2\sigma(I)$	$I > 2\sigma(I)$	$I > 2\sigma(I)$	$I > 2\sigma(I)$	$I > 2\sigma(I)$
R_{int}	0.027	0.022	0.039	0.051	0.042	0.022
θ_{max} (°)	27.4	27.5	27.5	27.4	27.5	27.5
Refinement						
Refinement on	F^2	F^2	F^2	F^2	F^2	F^2
$R[F^2 > 2\sigma(F^2)]$, $wR(F^2)$, S	0.024, 0.063, 1.08	0.016, 0.038, 1.03	0.028, 0.070, 1.05	0.029, 0.077, 1.12	0.029, 0.082, 1.03	0.027, 0.065, 1.02
No. of reflections	2310	2373	2367	2327	2390	2289
No. of parameters	127	170	136	136	136	136
H-atom treatment	Constrained to parent site	Constrained to parent site	Constrained to parent site	Constrained to parent site	Constrained to parent site	Constrained to parent site
Weighting scheme	$w = 1/[\sigma^2(F_o^2) + (0.0391P)^2]$, where $P = (F_o^2 + 2F_c^2)/3$	$w = 1/[\sigma^2(F_o^2) + (0.0168P)^2 + 0.2751P]$, where $P = (F_o^2 + 2F_c^2)/3$	$w = 1/[\sigma^2(F_o^2) + (0.0358P)^2 + 1.6942P]$, where $P = (F_o^2 + 2F_c^2)/3$	$w = 1/[\sigma^2(F_o^2) + (0.0454P)^2 + 0.1087P]$, where $P = (F_o^2 + 2F_c^2)/3$	$w = 1/[\sigma^2(F_o^2) + (0.0449P)^2 + 0.3505P]$, where $P = (F_o^2 + 2F_c^2)/3$	$w = 1/[\sigma^2(F_o^2) + (0.0435P)^2 + 0.0519P]$, where $P = (F_o^2 + 2F_c^2)/3$
$(\Delta/\sigma)_{max}$	0.001	0.002	0.001	<0.0001	0.001	0.001
$\Delta\rho_{max}$, $\Delta\rho_{min}$ (e Å⁻³)	0.28, −0.36	0.17, −0.20	0.67, −0.46	0.44, −0.32	0.51, −0.51	0.38, −0.73
Absolute structure	Flack (1983)	Flack (1983)	Flack (1983)	Flack (1983)	Flack (1983)	Flack (1983)
Flack parameter	0.010 (8)	−0.003 (7)		0.021 (11)		0.013 (10)

Computer programs used: *COLLECT* (Nonius BV, 1997–2000), *HKL SCALEPACK* (Otwinowski & Minor, 1997), *SHELXTL* (Sheldrick, 2008).

2.3. X-ray structural determinations

The crystals were prepared by dissolving 50 mg of each compound in 1 ml of ethanol at room temperature. The result was a two-phase system of liquids, consisting of the pure PBDE 3 or F PBDE 3 phase and a saturated ethanol solution of that compound. This two-layer liquid system was shock frozen in liquid nitrogen, followed by a partial thawing at 269 K. At least ten repeated cycles of partial thawing and subsequent cooling to 258 K resulted in excellent crystals. Special handling during crystal mounting was required because of the low melting points. A thin-walled Styrofoam

box (20 × 15 × 3 cm) was centered on the microscope stage with chunks of dry ice (1–2 cm in the maximum dimension) in each corner. Crystal handling tools were pre-cooled and kept in the box. When the temperature in the box equilibrated at approximately 253 K, the vials with crystals were transferred from the freezer into the box in a pre-cooled Dewar. Crystals were placed on a pre-cooled glass slide for inspection and selection. The selected crystal was adhered with paratone oil to a nylon loop attached to a pin mounted on a goniometer head (pin and loop were kept cold with dry ice). A small vial containing a piece of dry ice (also kept in the mounting box) was carefully slipped over the mounting pin to protect the crystal during transfer to the diffractometer. With the κ axis near its limit (so the φ axis points down), the goniometer head was attached and the protective vial removed, exposing the crystal to the cold nitrogen gas stream. Data were collected using standard CCD techniques. Structure determinations proved routine with SHELXTL programs. H atoms were located in difference maps, but were constrained with the riding model [C—H = 0.95 Å, $U_{iso}(H) = 1.2U_{iso,eq}(C)$]. For the 3-2F isomer, the late-stage difference Fourier maps suggested minor disorder of the flouro substituent. Refinement confirmed disorder via twofold rotation about the C1—C4 direction. The disorder was modeled as a whole-molecule disorder with the conformations constrained to be the same and partial atoms in close proximity (< 0.5 Å) constrained to have the same displacement parameters [e.g. $U_{aniso}(C1) = U_{aniso}(C'')$, $U_{aniso}(C2) = U_{aniso}(C6'')$, etc.]. F1'' was assigned $U_{iso}(F1'') = 1.2*U_{iso,eq}(C2'')$. The occupancy for the major site refined to 0.932 (2) (atoms at the minor site have labels with '' appended). Experimental details are given in Table 3. Ellipsoid plots are shown in Fig. 2. Bond lengths and angles fall within the expected ranges, see Table 2.

2.4. Database searches

Database searches were carried out on the November 2006 (with May 2007 update) version of the Cambridge Structural Database (CSD; Allen, 2002), with details in the supplementary material.

3. Results

3.1. Synthesis aspects

The synthesis of PBDE 3, $^{13}C_6$-PBDE and all five possible F-PBDEs 3 was carried out by nucleophilic substitution of the bromobenzene by a phenol under alkali conditions and is reported here for the first time. Briefly, the syntheses were carried out according to literature descriptions (Luthe, Leonards, Reijerink, Liu, Johansen & Robertson, 2006; Marsh et al., 1999, 2003). This synthesis method for low brominated PBDE analogues has the advantage of a one-step reaction with relatively high yields. We did not observe any conductive effect of the fluoro substituent. Best results were obtained by mixing the reactants in acetonitrile (Cristau et al., 2003), evaporating of the solvent under gentle warming and re-suspending the mixture in acetonitrile after 30 min
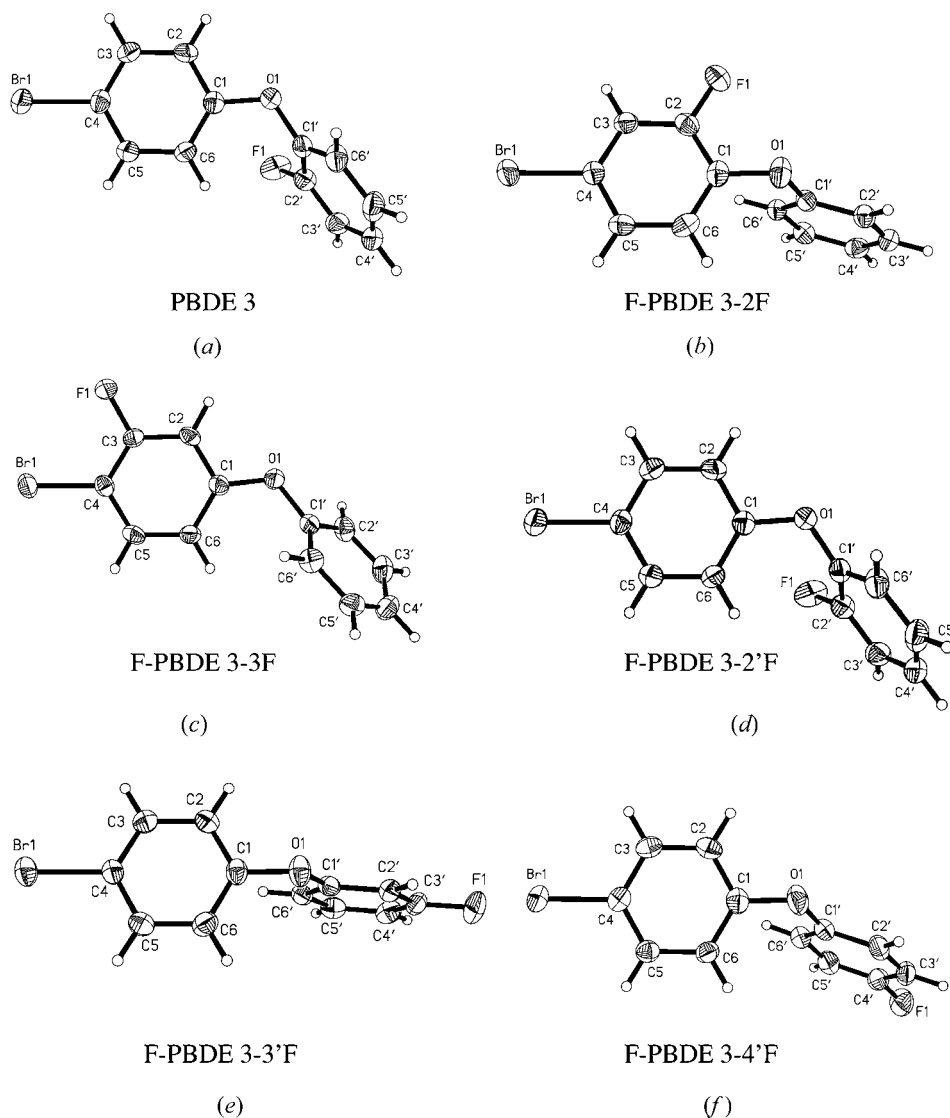
Figure 2
Ellipsoid plots (50% level) showing PBDE 3 and F-PBDEs 3: (a) 4-bromodiphenyl ether (PBDE 3), (b) 2-fluoro-4-bromodiphenyl ether (3-2F), (c) 3-fluoro-4-bromodiphenyl ether (3-3F), (d) 2'-fluoro-4-bromodiphenyl ether (3-2'F), (e) 3'-fluoro-4-bromodiphenyl ether (3-3'F) and (f) 4'-fluoro-4-bromodiphenyl ether (3-4'F).

Table 4
Torsion angles (°) ranges of mono-, di-, tri- and tetra-substituted diphenyl ethers, substituted by fluorine, chlorine, bromine and methyl in the *ortho* positions X_i ($i = 1$–4).

There are no mixed substitution patterns described. The torsion angles were determined by averaging the data for structures found in the Cambridge Structural Database and calculated by SCF-MO calculation (italics). For comparison, the torsion angles of diphenyl ether are 4.9, −175.0, 37.2, −147.5° (81, 16) for C1′—O—C1—C6 and C2′—C1′—O—C1, and 118.3 and 116.8° for C1—O—C1′. Note: First number in parenthesis is the number of structures found with the particular *ortho* substitution pattern. The second (bold) number in parenthesis refers to the iterations of the performed calculations. For the specific references, see supplementary materials.
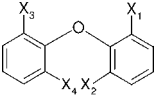
| | Torsion angles and bond angles of X_i substituted diphenyl ethers | | | | | | | | | | | |
| | C1′—O—C1—C6 | | | | C2′—C1′—O—C1 | | | | C1—O—C1′ | | | |
Substitution pattern	Fluoro	Chloro	Bromo	Methyl	Fluoro	Chloro	Bromo	Methyl	Fluoro	Chloro	Bromo	Methyl
X_1	11.3	1.9	96.7	113.2	78.0	99.1	8.5	145.5	119.8	119.0	117.9	117.8
					−108.34	−85.1	−172.7	−36.2				
	−43.7	*−42.6*	*−47.2*	*−39.6*	*152.4*	*153.1*	*149.1*	*149.1*	*116.6*	*116.4*	*116.5*	*116.7*
					−31.7	*−30.9*	*−35.5*	*−35.5*				
	(11, **32**)	(13, **37**)	(3, **9**)	(4, **16**)								
$X_1 X_2$	105.2	105.9	78.7	93.1	163.7	172.3	26.2	179.2	118.6	119.4	117.3	118.7
	−80.6	−78.6	−107.1	−91.2	−18.2	−10.3	−155.6	−0.1				
	94.8	*95.5*	*93.4*	*93.4*	*178.1*	*176.7*	*0.0*	*0.0*	*116.5*	*116.4*	*116.4*	*116.3*
	−93.1	*−91.6*	*−93.4*	*−93.4*	*−2.1*	*−3.8*	*180.0*	*180.0*				
	(4, **31**)	(1, **41**)	(4, **8**)	(3, **36**)								
$X_1 X_3$	–	−34.2	27.8	22.78	–	−34.2	50.0	90.4	–	119.9	118.6	118.6
		−34.2	50.0	−159.12		−34.2	50.0	90.4				
	−39.8	*−45.5*	*−44.5*	*−34.2*	*144.0*	*139.6*	*140.5*	*150.2*	*116.1*	*115.5*	*115.8*	*116.6*
	−40.9	*−45.5*	*−44.5*	*−42.3*	*145.1*	*139.6*	*140.5*	*142.9*				
	(0, **58**)	(3, **21**)	(3, **47**)	(1, **57**)								
$X_1 X_2 X_3$	–	–	–	–	–	–	–	–	–	118.81	115.67	–
	–	–	–									
	98.7	*105.5*	*106.8*	*96.0*	*121.1*	*158.8*	*160.5*	*162.5*	*114.7*	*115.9*	*116.2*	*116.1*
	−88.4	*−81.7*	*−80.2*	*−90.7*								
	(0, **89**)	(0, **15**)	(0, **9**)	(0, **43**)								
$X_1 X_2 X_3 X_4$	57.7	–	39.0	–	57.7	–	39.0	–	117.7	–	120.9	–
	−127.7		−146.4		−128.0		−146.4					
	64.0	*56.0*	*54.9*	*53.1*	*64.0*	*56.0*	*54.9*	*53.1*	*116.3*	*117.8*	*118.8*	*118.1*
	−123.3	*−131.3*	*−132.6*	*−133.7*	*−123.3*	*−131.3*	*−132.6*	*−133.7*				
	(23, **18**)	(0, **9**)	(2, **10**)	(0, **44**)								

of dryness. Extended heating under dry conditions should be avoided since it results in de-bromination and a scrambling of the bromo substituent. The overall yields were increased by applying repeated cycles of short dryness, re-suspension in acetonitrile and refluxing.

3.2. C—F and C4—Br bond lengths and Br—C4—C3, Br—C4—C5 and F—C—C angles

With a few exceptions, the observed bond lengths C—F and C4—Br, and bond angles Br—C4—C3, Br—C4—C5 and F—C—C are comparable to those of the calculated molecules within the study compounds. The C—Br bond lengths are statistically the same [1.896 (3)–1.904 (2) Å] with the exception of the 3-3F isomer [C—Br = 1.880 (3) Å], where the Br and F substituents are vicinal. This effect was not seen in the calculated model. The C—F bond lengths of the *ortho*-substituted 3-2F and 3-2′F are the shortest with 1.349 (1) and 1.347 (2) Å (1.351 Å calculated), while 3-3′F has the longest C—F bond of 1.362 (2) Å (1.355 Å calculated). The Br—C4—C3 and Br—C4—C5 bond angles are widened by 1–2° up to 121.0 (2) and 121.1 (2)° (122.8° calculated) in the 3-3F isomer (vicinal fluoro substituent). The repulsion between the bromine and fluorine substituents is demonstrated by the

bond angles F—C3—C2 [117.7 (2)° observed, 118.0° calculated] and F—C3—C4 [119.4 (2)° observed, 121.6° calculated] of the 3-3F isomer. The observed distortion is smaller than the calculated one.

3.3. C—C and C—O bond lengths and angles

The calculated and observed C—C bond lengths and interior angles are generally in good agreement and are of similar magnitude, see Table 2. Exceptions are the changes in the C—C bond lengths and interior angles by fluoro substitution in the phenyl rings. Effects of fluoro substitution could be observed by X-ray, but were not calculated. The fluoro-*ipso* bond angles are increased: 121.95 (10)° in 3-2F, 121.9 (2)° in 3-2′F, 122.9 (2)° in 3-3F, 124.0 (2)° in 3-3′ and 122.2 (3)° in 3-4′F, compared with the nominal angle of 120.2 (2)° (PBDE 3). The other interior angles decreased slightly. The calculation model did not predict this effect, see Table 2.

The X-ray determinations show that the steric and electronic influence of fluorine has some effect on the C1—O and C1′—O bond lengths. In the 3-3F isomer, the C—O bond is shorter in the ring carrying the fluorine, *i.e.* 1.364 (3) (C1—O) *versus* 1.410 (3) Å (C1′—O). The bond angles of C6—C1—O, C2—C1—O, C6′—C1′—O and C2′—C1′—O follow the

distortion of the interior angles of the aromatic ring by fluoro substitution. The C6—C1—O and C6′—C1′—O bond angles are reduced by *ortho*-fluoro substitution to 120.80 (14) (3-2F) and 119.48 (18)° (3-2′), and increased by *meta*-fluoro substitution to 126.3 (2) (3-3F) and 123.73 (18)° (3-3′F) compared with the nominal angles of 124.4 (2) and 122.8 (2)° (PBDE 3). The C2—C1—O and C2′—C1′—O bond angles are increased for *ortho* substitutions to 119.93 (13) (3-2F) and 121.24 (19)° (3-2′F) and decreased for the *meta* positions to 114.2 (2) (3-3F) and 114.19 (17)° (3-3′F) compared with 115.4 (2) and 116.1 (2)° (PBDE 3). As was the case with the interior angles, the calculation model did not correctly predict the influence of fluoro substitution, see Table 2.

3.4. Torsion and C—O—C bond angles

In general, the observed torsion angles C1′—O—C1—C6(2) and C2′(6′)—C1′—O—C1, and the calculated values for the series of PBDE 3 and F-PBDEs 3 are similar. PBDE 3 and all F-PBDEs 3 have a twisted conformation, see Table 2. However, no trend was found for observed and calculated torsion angles of the PBDE/F-PBDEs 3 congeners.

Comparing diphenyl ether with mono- to tetra-fluoro, chloro, bromo or methyl substitutions in the *ortho* positions, we observed a general agreement between the calculated and observed torsion angles (see Table 4). The closest agreement between observed and calculated data was seen for the mono-substituted congener *ortho*-methyldiphenyl ether (observed: 145.5, −36.2°; calculated: 149.1, −35.5°). This trend continued for all higher methyl-substituted congeners. For the di-substituted congeners, good agreement can also be observed for the difluorodiphenyl ether (observed: 163.7, −18.2°; calculated: 178.1, −18.2°) and all other di- to tetra-substituted halo-analogues. Two exceptions were trichlorodiphenyl ether (observed: −5.1°; calculated: 158.8°) and tribromodiphenyl ether (observed: 26.3°; calculated: 160.5°).

We observed that the C1—O—C1′ bond angle in 3-2F displayed the smallest value [115.96 (12)°], and was largest for PBDE 3 [121.09 (18)°] and 3-3F [120.9 (2)°]. When comparing the C1—O—C1′ angle in diphenyl ethers with mono- to tetra-fluoro, chloro, bromo and methyl substitutions in the *ortho* positions, we observed a trend in the calculated values of the increased angle with a higher degree of substitution and increasing volume of the substituent (see Table 4). This trend was not observed in the corresponding crystal structures. This might be due to the limited number of structures for these types of compounds.

3.5. Packing of the PBDE 3 and F-PBDEs 3 isomers

The intermolecular interactions of BDE3 and the F-BDE3 isomers are weak and primarily C-H(F, Br)···π with some C—H···F interactions, see Fig. 3. No close halogen–halogen contacts were noted. In each structure the molecules stack to form columns in the direction of the shortest unit-cell vector. (Note: for each structure below, $X1a$ = centroid of the C1–C6 phenyl ring and $X1b$ = centroid of the C1′–C6′ phenyl ring.)

3.5.1. Packing of the 4-bromodiphenyl ether (PBDE 3). The columns are interconnected *via* C—H···π interactions to form sheets perpendicular to the *a* axis [H2···$X1a^i$ = 2.880 Å, H5···$X1a^{ii}$ = 2.745 Å, H2′···$X1b^{iii}$ = 2.939 Å, H5′···$X1b^{iv}$ = 2.863 Å; (i) $x, 2 - y, -\frac{1}{2} + z$; (ii) $x, 1 - y, \frac{1}{2} + z$; (iii) $x, 1 - y, -\frac{1}{2} + z$; (iv) $x, 2 - y, \frac{1}{2} + z$]. The sheets interact *via* van der Waals forces with a close C3′—H3′···Br^v contact [0.95, 3.00, 3.566 Å, 145°; (v) $\frac{1}{2} + x, \frac{3}{2} - y, -\frac{1}{2} + z$].

3.5.2. Packing of the 2-fluoro-4-bromodiphenyl ether (3-2F). C—H···π [H4′···$X1a^i$ = 2.936 Å, H5···$X1b^{ii}$ 2.875 Å; (i) $x, -1 + y, z$; (ii) $1 - x, \frac{1}{2} + y, \frac{3}{2} - z$] and C—Br···π [Br1···$X1a^{iii}$ = 3.761 Å, (iii) $2 - x, \frac{1}{2} + y, \frac{3}{2} - z$] interactions connect the columns into bilayers with the F atoms on the exterior of the bilayers. C—H···π interactions [H2′···$X1b$(iv) = 3.001 Å, (iv) $-\frac{1}{2} + x, \frac{1}{2} - y, 2 - z$] connect the bilayers. The van der Waals forces hold the bilayer together.

3.5.3. Packing of the 2′-fluoro-4-bromodiphenyl ether (3-2′F). C—H···π, C—F···π and C—H···F interactions connect the molecules in the columns [H2···$X1a^i$ = 3.384 Å, H5···$X1a^{ii}$ = 3.386 Å, H5′···$X1b^{ii}$ = 3.498 Å, F1···$X1b^i$ = 3.473 Å and C6—H6···F1^{iii} 0.95, 2.43, 3.256 (3) Å, 145°; (i) $x, -1 + y, z$; (ii) $x, 1 + y, z$; (iii) $x, 1 + y, z$] and interconnect neighboring columns [C5—H5···F1^{iv} 0.95, 2.48, 3.375 (3) Å, 157°; (iv) $1 - x, 1 + y, \frac{1}{2} - z$] to double the columns. The doubled columns are held together *via* van der Waals forces.

3.5.4. Packing of the 3-fluoro-4-bromodiphenyl ether (3-3F). The columns interconnect *via* C—H···π and C—H···F interactions forming a three-dimensional network [H2···$X1a^i$ 2.710 Å, H5···$X1a^{ii}$ 2.839 Å, H5′···$X1b^{iii}$ 2.943 Å, H2′···$X1b^{iv}$ 3.380 Å and C4′—H4′···F1^v 0.95, 2.42, 3.239 (3) Å, 145°; (i) $-x, 1 - y, -\frac{1}{2} + z$; (ii) $\frac{1}{2} - x, y, \frac{1}{2} + z$; (iii) $-x, 2 - y, \frac{1}{2} + z$; (iv) $\frac{1}{2} - x, y, -\frac{1}{2} + z$; (v) $x, 1 + y, z$].

3.5.5. Packing of the 3′-fluoro-4-bromodiphenyl ether (3-3′F). The columns interconnect *via* C—H···π and C—Br···π interactions forming a three-dimensional network [H4′···$X1a^i$ = 3.064 Å, Br1···$X1a^{ii}$ = 3.714 Å, H2···$X1b^{iii}$ = 2.732 Å, H5···$X1b^{iv}$ = 2.890 Å; (i) $x, -1 - y, z$; (ii) $\frac{1}{2} - x, \frac{1}{2} + y, \frac{3}{2} - z$; (iii) $1 - x, 1 - y, 1 - z$; (iv) $\frac{3}{2} - x, \frac{1}{2} + y, \frac{3}{2} - z$; (v) $x, 1 + y, z$].

3.5.6. Packing of the 4′-fluoro-4-bromodiphenyl ether (3-4′F). The columns interconnect *via* C—H···π, C—F···π and C—Br···π interactions forming a three-dimensional network [H5···$X1a^i$ = 3.243 Å, Br1···$X1a^{ii}$ = 3.735 Å, Br1···$X1b^{iii}$ = 3.461 Å, F1···$X1b^{iv}$ = 3.469 Å; (i) $x, -y, -\frac{1}{2} + z$; (ii) $\frac{1}{2} + x, \frac{1}{2} + y, z$; (iii) $-\frac{1}{2} + x, \frac{1}{2} + y, z$; (iv) $\frac{1}{2} + x, \frac{1}{2} - y, -\frac{1}{2} + z$].

4. Discussion

4.1. Synthesis aspects

Several pathways to obtain the desired PBDE 3 and analogues are described in the literature, *i.e.* coupling of diphenyl iodyl salts with phenols (Luthe, Leonards, Reijerink, Liu, Johansen & Robertson, 2006, Marsh *et al.*, 1999, 2003), coupling of arylboronic acids with phenols (Chouteau *et al.*, 2005), ether synthesis by Ullmann coupling (Luthe, Leonards, Reijerink, Liu, Johansen & Robertson, 2006; Qian *et al.*, 2003; Cristau *et al.*, 2003) and direct substitution of the diphenyl

ether molecule or its derivatives (Luthe, Leonards, Reijerink, Liu, Johansen & Robertson, 2006). PBDE 3 was synthesized by several methods independently. The highest yield of 98% was obtained by using *N*-bromo-succinimide and ammonium nitrate in acetonitrile. The syntheses of the five F-PBDEs 3 are reported here for the first time. Owing to the commercial availability of the starting materials, the short synthetic pathway of a single reaction step, the high purity of the products and the relatively high yields (> 90%; Cristau *et al.*, 2003), we employed Ullmann coupling. In addition to these advantages, the fluoro substituent has no conductive influence on the reaction, as it does in a direct coupling with diphenyl iodyl salts (Luthe, Leonards, Reijerink, Liu, Johansen & Robertson, 2006). The yields obtained are competitive: PBDE

(a)

(b)

(c)

(d)

(e)

(f)
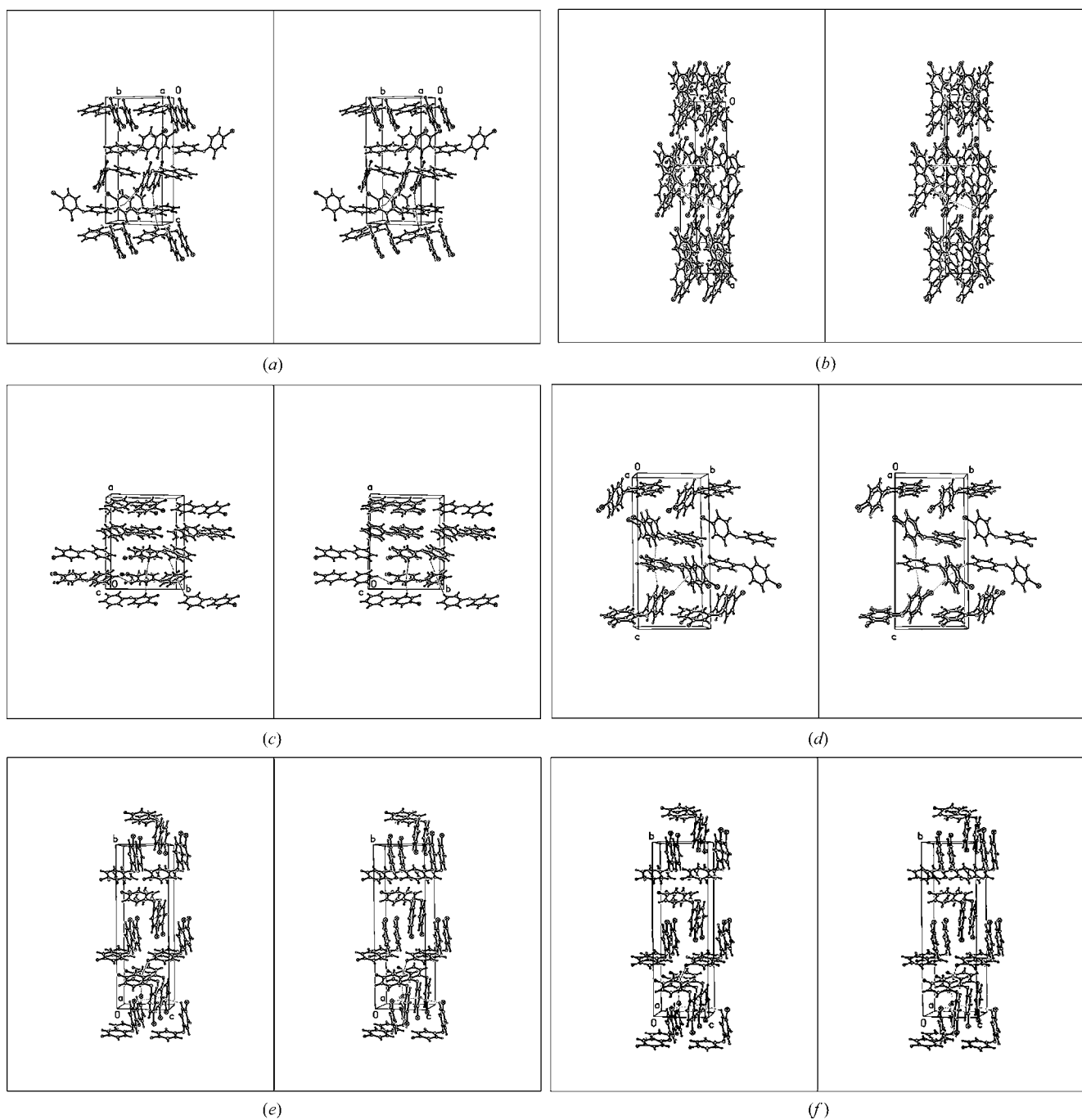
Figure 3
Stereodiagrams of unit-cell contents showing intermolecular interactions (dotted lines). Atoms are shown as spheres of arbitrary size with the highest atomic number having the largest radius and the lowest the smallest. (*a*) 2-Fluoro-4-bromodiphenyl ether (3-2F), (*b*) 2′-fluoro-4-bromodiphenyl ether (3-2′F), (*c*) 3-fluoro-4-bromodiphenyl ether (3-3F), (*d*) 3′-fluoro-4-bromodiphenyl ether (3-3′F), (*e*) 4′-fluoro-4-bromodiphenyl ether (3-4′F) and (*f*) 4-bromodiphenyl ether (PBDE 3).

3 (59%), $^{13}C_6$-PBDE 3 (60%), 3-2F (54%), 3-3F (55%), 3-2'F (59%), 3-3'F (60%) and 3-4'F (58%). The synthesis conditions are responsible for the somewhat lower yields for the congeners 3-2F and 3-3F. With a large excess of the bromobenzene, the side reaction of self-attack can be reduced, resulting in a higher product yield. We observed that the solvent volume was critical for the successful reaction.

4.2. H, ^{13}C and ^{19}F NMR and MS characterization

The ^{1}H NMR spectra of the PBDE 3 and F-PBDEs 3 are of higher spin order. Determinations of the shifts and couplings were carried out using ^{1}H ^{13}C COSY NMR, see the supplementary material. The PBDE 3 carrying the bromine is an A,A',X,X' and an $A,A'X,X',Z$ system (prime side); 3-2F is an A,B,Z and an $A,A'X,X',Z$ system (prime side); 3-2'F is an A,A',X,X' and A,B,X,Z system (prime side); 3-3F is an A,X,Z and A,A',X,X',Z system (prime side); 3-3'F is an A,A',X,X' and A,B,X,Z system (prime side) and 3-4'F is an $A,A'X,X'$ and A,A',Z' system (prime side). The chemical shifts are between δ = 6.69 (3-3F) and 7.77 p.p.m. (3-3'F). Protons vicinal to the fluoro substitution are shifted to higher δ values, and those in the *meta* positions to lower values. Fluoro substitution also influenced the electron density on the ring not carrying a fluorine and changed the ^{1}H chemical shifts slightly, *i.e.* from 6.89 p.p.m. for H2/6 to 6.87 p.p.m. (3-2'F), 6.94 p.p.m. (3-3'F) and 6.83 p.p.m. (3-4'F), for H3/5 from 7.43 to 7.48 p.p.m. (3-3'F) and 7.41 p.p.m. (3-4'F), for H2'/6' from 7.00 to 7.03 p.p.m. (3-3F). The J_{HH} couplings are between $^3J_{HH}$ 7.4 and 9.00 Hz, $^4J_{HH}$ 1.0 and 2.4 Hz. Bromo substitution as well as oxygen substitution increased the coupling strength, *e.g. cf.* $^4J_{H3'H5'}$ 1.0 Hz with $^4J_{H3H5}$ 2.2 Hz *via* bromine in 3-2F and $^4J_{H3'H5'}$ 1.0 Hz with $^4J_{H2H6}$ 2.7 Hz *via* oxygen in 3-3F. Fluoro substi-

tution influenced the coupling strength of its neighbor's protons as well, but not in the *ortho* position as in the case of the bromo substituent, but in the *meta* position. For example, 3-2'F showed a coupling of $^4J_{H,H}$ 2.4 Hz *versus* 2.0 Hz in a non-substituted ring.

^{13}C NMR spectra (see Table 1) show higher chemical shifts [ranging from 143.3 (3-2'F) to 158.5 p.p.m. (3-3F and 3-3'F)] for the C1/1' positions due to the negative inductive effect of oxygen on C atoms with *ipso*-O substitution. Comparing the shifts induced by a *meta*-fluoro substitution in C3/3' shows the electron density increasing by *ortho*-bromo substitution, resulting in a lower shift of 159.7 p.p.m. (3-3F) *versus* 163.7 p.p.m. (3-3'F). The $^1J_{CF}$ couplings ranged from 242.28 to 253.60 Hz. The strength of the coupling reflects the strength of the C—F bond. The C2/2' positions have the highest electron density based on the ^{13}C NMR shifts and the $^1J_{CF}$ of the *ortho*-fluoro substituents is the strongest, with 253.6 (3-2F) and 249.07 Hz (3-2'F). Similar conclusions can be drawn based on the electron density of the F—C bonds for $^2J_{CF}$ couplings. To determine the change in electron density by fluoro substitution, the difference between the ^{13}C NMR shifts of a given substituted compound (F-PBDEs 3) and the corresponding parent compounds (PBDE 3) were calculated, see Fig. 4. Positive values indicate an increase in electron density, negative values indicate a decrease. As expected, the C atoms *ortho* to the F substituent show the largest increase in electron density with a smaller increase at the C atom *para* to the F substituent. This information is critical for understanding the shape and reactivity of the cogeners and is therefore of fundamental importance.

The ^{19}F NMR spectra are of first order and can be explained on the basis of direct coupling with its neighboring H atoms. The chemical shifts (see supplementary material) in the ^{19}F NMR spectrum are the highest for the positions C3, 5 and 4' with -104.64 p.p.m., followed by C3' and 5' with -110.84 p.p.m., C2 and 6 with -128.05 p.p.m. and finally C2' and 6' with -130.68 p.p.m. The C4 (^{13}C δ 115.8 p.p.m.) has the highest electron density due to the bromo substituent, followed by C2' and 6' (^{13}C δ 119.2 p.p.m.), C2 and 6 (^{13}C δ 120.6 p.p.m.), C3' and 5' (^{13}C δ 130.1 p.p.m.), C3 and 5 (^{13}C δ 132.9 p.p.m.), see Table 1.

The ^{19}F NMR δ shift -119.55 p.p.m. of C4' cannot be explained on the basis of electron density alone, since the ^{13}C δ 123.9 p.p.m. should result in a ^{19}F δ of about -125 p.p.m. We explain this anomaly on the basis of the magnetic anisotropy effect. The J_{FH} couplings are strong. $^3J_{FH}$ couplings range from 8.0 to 10.00 Hz, $^4J_{FH}$ 4.6–8.4 Hz, $^5J_{FH}$ 1.1–1.5 Hz. The ^{19}F NMR spectra of 3-2'F is non-symmetrical. Since ^{1}H–^{19}F coupled spin systems cannot lead to spectra of second or higher order, this observation can be explained on the basis of signal carryover and more than one signal coincidently resonating at the same frequency. The proton-coupling partners are not magnetically equivalent.

The parent ion peak $[M]^{+\cdot}$ is the main signal in MS for PBDE 3 and the corresponding F-PBDEs 3. Major fragments are $[M-Br]^+$, $[M-HBr]^{+\cdot}$, $[M-C_2Br]^+$, $[M-C_2H_2Br]^{+\cdot}$ and $[M-C_2H_4Br]^{+\cdot}$. Fluorine loss is around 1% and reflects the strong
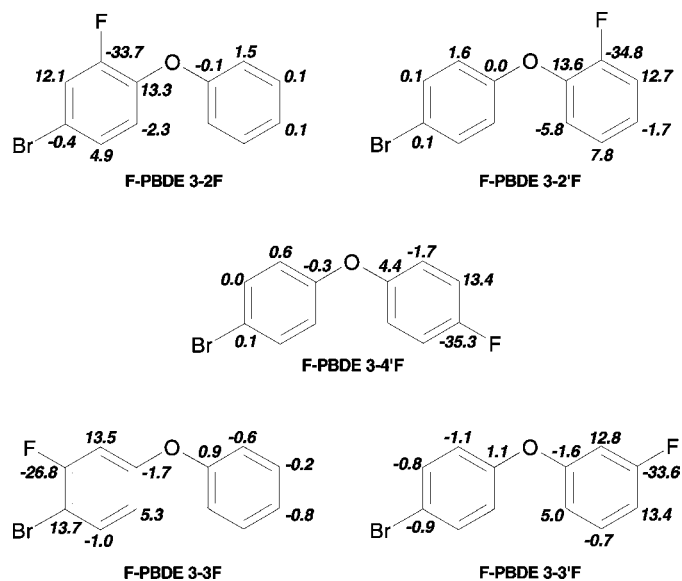
Figure 4
Changes in the ^{13}C NMR shifts, δ (p.p.m.) by fluorine substitution relative to PBDE 3 (4-bromodiphenyl ether). ^{13}C NMR shifts indicate a change in electron density at the C atom. Positive values indicate an increased electron density, negative values a decrease. For more details see §2.

C—F bond, especially in an aromatic system due to hyper-conjugation. The $[M]^{++}$ reflects the potential to stabilize a second positive charge of the molecule by delocalization or resonance. For PBDE 3 the abundance of the $[M]^{++}$ is only 1%, but increases by mono-fluorination to 14% (for 3-2F), 16% (for 3-3F, 3-3′F and 3-4′F) and 24% (for 3-2′F). A similar observation was made comparing mono-fluorinated polycyclic aromatic hydrocarbons with their non-fluorinated parent compounds (Luthe *et al.*, 2003). The electron density in a π-bond system diminishes with fluoro substitution, but increases *via* hyperconjugation in a π-bond system since fluorine is too 'hard' to retain the charge and pushes it back *via* p-π-orbital overlap. This results in a stabilization of the additional charge. This charge stabilization is also reinforced by the negative inductive effect of fluorine, as the removal of a second electron would lead to a less energetic atomic orbital $1s^2 2s^2 2p^4$, with two unpaired electrons for fluorine.

4.3. C—F and C4—Br bond lengths

The differences in C—F and C—Br bond lengths may be explained on the basis of differences in electron density and orbital overlap. Many factors, *e.g.* mesomeric, inductive, steric and/or direct electric field effects, may alter the electron density. Substituent-induced chemical shifts in the ^{13}C NMR spectrum reflect the actual distribution of electrons at the C atom. We have utilized ^{13}C NMR measurements to indicate alterations in the electron density of the C atoms. Fig. 4 gives an overview of the relative change of electron density for the C positions 1–6, and 1′–6′ as a result of fluoro substitution compared with PBDE 3. In the ^{13}C NMR, higher shift values indicate a reduction in electron density at the C atom, lower ones an increase. Therefore, positive relative values in Fig. 4 indicate an increase of electron density and negative ones a decrease. A lower electron density results in a weaker and therefore longer C—F bond. In the unsubstituted ring of F-PBDE 3-3′F, the C3′ (the *meta* position) has the strongest ^{13}C NMR shift δ of 1163.7 p.p.m. and shows the longest C—F bond of the F-PBDEs 3 [1.362 (2) Å]. Comparing the shifts for C1′–C6′ in PBDE 3 with C1–C6 in diphenyl ether demonstrates that the bromine has a negligible effect on the non-bromo-substituted ring in PBDE 3. In the Br-substituted ring of PBDE 3, the highest ^{13}C NMR shift δ of 132.9 p.p.m. (*meta* position) results in the longest C—F bond of 1.357 (3) Å at the C3 position. The strength of the J_{CF} couplings does not follow the trend of the C—F bond lengths, see Fig. 5. We found in general that a strong coupling results in a shorter bond, but the values determined for the specific isomers do not reflect the trend in bond length. Aside from the electron density of the carbon, buttressing effects, electron donation and withdrawing over space, and steric effects also play a major role. Differences in the C—F bond lengths could also be calculated using SCF-MO methods.

With the exception of the 3-3F isomer, there is no significant trend in the C4—Br bond lengths observed, nor do the calculated C—Br bond lengths show any significant differences between the isomers. The short C4—Br bond

[1.880 (3) Å] is found in the 3-3F isomer where the halo substutients are vicinal. This does correlate with electron density, as determined by ^{13}C NMR for this C4 position. The change of electron density in the F-PBDEs 3 relative to PBDE 3 at the various positions is indicated by the chemical shift and relative chemical shift of the position. The relative shift is found by subtracting the ^{13}C NMR shifts of the F-PBDEs 3 from the corresponding shift of PBDE 3, see Fig. 4. For the C4 position the 3-3F isomer has the smallest shift (102.1 p.p.m.) and therefore the biggest relative shift (13.7 p.p.m.). This can be accounted for by *ortho* induction. The range of shifts for C4 in PBDE3 and the other isomers is small (115.7–16.7 p.p.m.). This correlates with the lack of a significant difference [1.896 (3)–1.904 (2) Å] in the C—Br bond length of these isomers. The influence of the fluoro substitution on the C4—Br bond length could not be calculated using AM1.

4.4. Influence of fluoro substitution on aromatic interior bond angles

X-ray analysis, rotational spectroscopy and SCF-MO calculations all showed a distorted ring in fluorobenzene (Oosaka & Akimoto, 1953). As discussed earlier (Luthe, Swenson & Robertson, 2007), this is explained by hyperconjugation of the $2p$ orbitals of the fluoro substituent with the aromatic π system. In chloro- and bromobenzene, this effect was not observed since the $3p$ and $4p$ orbitals are too big to result in a good overlap with the aromatic π system. The fluoro-*ipso* bond-angle increase ranged from 121.9 (2) to 124.0 (2)° and the adjacent angles decreased [ranging from 117.2 (2) to 119.24 (13)°]. No significant influence to this *ipso* angle increase was found in the other ring angles. We were able to model this *ipso* effect by calculation. No attraction of the fluoro and bromo substituents towards each other in the vicinal positions (3-3F) was observed, although it was observed in chloro–fluoro-substituted aromatic systems (Luthe, Swenson & Robertson, 2007). This is likely due to little or no overlap of the $2p$ and the $4p$ orbitals of the vicinal fluoro and the bromo substitutents. A more detailed study regarding this intriguing aspect is in progress.

4.5. Influence of fluoro substitution on the torsion angles φ_1 and φ_2

We compared the torsion angles C1′—O—C1—C6(2) and C2′(6′)—C1′—O—C1, and the bond angle C1—O—C1′ in diphenyl ether with fluoro, chloro, bromo and methyl, and no
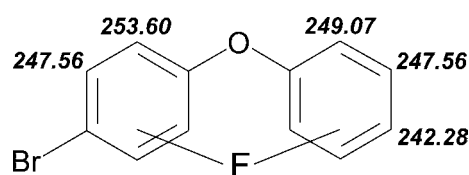
Figure 5
Direct carbon–fluorine couplings, J_{CF} (Hz) in all F-PBDEs 3. Stronger couplings relate to a higher electron density in the C—F bond.

substitution in the *ortho* positions, see Table 4. We observed that in general there is agreement of calculated and observed data. The conformity depends on the size of the substituent, the degree of substitution and the position. Mono substitution by a methyl function resulted in good agreement (observed: 145.5, −36.2°; calculated: 149.1, −35.5°). For fluoro substitution (the smallest substituent in the comparison study), agreement began with difluorodiphenyl ether (observed: 163.7, −18.2°; calculated: 178.1, −18.2°) and continued with higher degrees of substitution.

The average angle of the ether linkage in the study compounds was 118.8 (46)°, resulting in an average distance of C1···C1′ of 2.39 Å. This distance is 0.91 Å longer than the 1.48 Å in PCBs (Luthe, Swenson & Robertson, 2007) and results in a weaker steric interaction between the *ortho* substituents. The ether bond and the C1—O—C1′ angle both contribute to the flexibility of the substituted diphenyl ethers, which helps minimize steric interaction between the phenyl rings. Therefore, the steric interaction must be strong enough because of the size of the substituent, and the degree and pattern of substitution to emphasize the intramolecular steric interaction over the energy gained from weak intermolecular interactions in the solid state, *e.g.* stacking effects and C—H(F, Br)···π interactions. The steric interactions for this series are too weak to give a clear picture of the intramolecular interactions, even though the solid-state intermolecular interactions of PBDE 3 and the F-PBDE 3 isomers are weak C—H(F,Br)···π and C—H···F interactions.

4.6. Packing of the F-PBDEs 3 isomers

The intermolecular interactions for PBDE 3 and all five F-PBDE 3 isomers are dominated by weak C—H(F,Br)···π and C—H···F interactions, whereas the F-PCBs 3 are dominated by π···π stackings. This leads to crystal packings built up by columns along the shortest unit-cell vector, which are interconnected *via* C—H(F,Br)···π interactions, C—H···F(Br) close contacts and van der Waals forces. The 3-3′F and 3-4′F have very similar crystal packing interactions. The 3-2F isomer has stacks connected into bilayers with the F atoms on the exterior of the bilayers. There are no linear halo···halo interactions, *e.g.* F···Br, as could be found for F···Cl in F-PCBs. This is likely due to the large differences of the orbital sizes.

References

Allen, F. H. (2002). *Acta Cryst.* B**58**, 380–388.

Ballschmiter, K. Z. & Zell, M. (1980). *Fresenius Z. Anal. Chem.* **302**, 20–31.

Bergman, Å., Athanasiadou, M., Wehler, E. K. & Sjödin, A. (1999). *Organohalogen Compd,* **43**, 89–92.

Bromine Science & Environmental Forum (2003). Total Market Demand, http://www.bsef.com.

Choudhury, A. R., Islam, K., Kirchner, M. T., Mehta, G. & Guru Row, T. N. (2004). *J. Am. Chem. Soc.* **126**, 12274–12275.

Chouteau, F., Ramanitrahasimbola, D., Rasoanaivo, P. & Chibale, K. (2005). *Bioorg. Med. Chem. Lett.* **15**, 3024–3028.

Cristau, H.-J., Cellier, P. P., Hamada, S., Spindler, J.-F. & Taillefer, M. (2003). *Org. Lett.* **6**, 913–916.

Dewar, M. J. S., Zoebisch, E. G., Healy, E. F. & Stewart, J. J. P. (1985). *J. Am. Chem. Soc.* **107**, 3902–3909.

Flack, H. D. (1983). *Acta Cryst.* A**39**, 876–881.

Hites, R. (2004). *Environ. Sci. Technol.* **38**, 945–956.

Hites, R. A., Foran, J. A., Schwager, S. J., Knuth, B. A., Hamilton, M. C. & Carpenter, D. O. (2005). *Environ. Sci. Technol.* **39**, 379–380.

Johanson-Restrepo, B., Kannan, K. & Raport, D. P. (2005). *Environ. Sci. Technol.* **39**, 5177–5182.

Lind, Y., Aune, M., Atuma, S., Becker, W., Bjerselius, R., Glynn, A. & Darnerud, P. O. (2002). *Organohalogen Compd,* **58**, 181–184.

Luthe, G., Ariese, F. & Brinkman, U. A. Th. (2002). *Handbook of Environmental Chemistry: Organic Fluorine Compounds*, edited by A. H. Neilson, pp 249–275. Berlin: Springer Verlag.

Luthe, G., Jacobus, J. & Robertson, L. W. (2007). *Environ. Toxicol. Pharmacol.*, doi: 10.1016/j.etap.2007.10.1017.

Luthe, G., Leonards, P. E., Reijerink, G. S., Liu, H., Johansen, J. E. & Robertson, L. W. (2006). *Environ. Sci. Technol.* **40**, 3023–3029.

Luthe, G., Ramos, L., Dalluege, J. & Brinkman, U. A. Th. (2003). *Chromatographia,* **57**, 379–384.

Luthe, G., Schut, B. G., Aaseng, J. E. & Johansen, J. E. (2006). *Chemosphere* **64**, 250–255.

Luthe, G., Swenson, D. C. & Robertson, L. W. (2007). *Acta Cryst.* B**63**, 319–327.

Marsh, G., Hu, J., Jakobsson, E., Rahm, S. & Bergman, Å. (1999). *Environ. Sci. Technol.* **33**, 3033–3037.

Marsh, G., Stenutz, R. & Bergman, Å. (2003). *Eur. J. Org. Chem.* **14**, 2566–2576.

Meironyte, D., Noren, K. & Bergman, A. (1999). *J. Toxicol. Environ Health A,* **58**, 329–341.

Nevalainen, T. & Rissanen, K. (1994). *J. Chem. Soc. Perkin Trans. 2,* pp. 271–279.

Nonius (1997–2000). *COLLECT.* Nonius BV, Delft, The Netherlands.

Nordic Council of Ministers (1998). *Polybrominated Diphenyl Ethers: Food Contamination and Potential Risks.* Report from an NNT Project Group, p. 503. TemaNord, Copenhagen, Denmark.

Otwinowski, Z. & Minor, W. (1997). *Methods in Enzymology*, Vol. 276, *Macromolecular Crystallography*, edited by C. W. Carter Jr & R. M. Sweets, Part A, pp. 307–326. New York: Academic Press.

Oosaka, H. & Akimoto, Y. (1953). *Bull. Chem. Soc. Jpn,* **26**, 433–438.

Qian, D.-Q., Shine, H. J., Thurston, J. H. & Whitmire, K. H. (2003). *J. Phys. Org. Chem.* **16**, 142–147.

Schaefer, T., Penner, G. H., Takeuchi, C. & Tseki, P. (1988). *Can. J. Chem.* **66**, 1647–1650.

Shao, Y. *et al.* (2006). *Phys. Chem. Chem. Phys.* **8**, 3172–3192.

Sheldrick, G. M. (2008). *Acta Cryst.* A**64**, 112–122.

Sjödin, A., Carlsson, H., Thursesson, K., Sjolin, S., Bergman, A. & Ostman, C. (2001). *Environ. Sci. Technol.* **35**, 448–454.